H35,54

copy 2

NACA

RESEARCH MEMORANDUM

JUN 26 1947

PRESSURE-DISTRIBUTION MEASUREMENTS ON A FULL-SCALE

HORIZONTAL TAIL SURFACE FOR A MACH NUMBER RANGE

OF 0.20 TO 0.70

By

Carl F. Schueller

Langley Memorial Aeronautical Laboratory
Langley Field, Va.

NATIONAL ADVISORY COMMITTEE
FOR AERONAUTICS

WASHINGTON

June 25, 1947

3 1176 01436 3445

NATIONAL ADVISORY COMMITTEE FOR AERONAUTICS

RESEARCH MEMORANDUM

PRESSURE-DISTRIBUTION MEASUREMENTS ON A FULL-SCALE

HORIZONTAL TAIL SURFACE FOR A MACH NUMBER RANGE

OF 0.20 TO 0.70

By Carl F. Schueller

SUMMARY

Tests of a full-scale, semispan, horizontal tail surface for a jet-propelled fighter airplane have been conducted in the Langley 16-foot high-speed tunnel to determine the variation of the chordwise and spanwise pressure distributions with Mach number.

Surface irregularities were found to cause appreciable distortion of the pressure distribution. The highest critical speed of the tail surface was 0.77. By elimination of the surface irregularities, it is estimated that this could be increased to 0.80.

The rate of change of pressure coefficient with angle of attack over the leading 60 percent of the chord increased with increasing Mach number due to compressibility effects while no systematic variation was apparent aft of the hinge line. The rate of change of pressure coefficient with elevator angle decreased over the leading 15 percent of the tail surface as a result of model twist and increased at the 70-percent and 77-percent chord stations with increasing Mach number.

Reasonable agreement between the calculated and experimental root-bending-moment coefficient was obtained up to a Mach number of 0.68.

INTRODUCTION

A full-scale, semispan, horizontal tail surface of a jet-propelled fighter-type airplane was tested to determine its aerodynamic characteristics at Mach numbers in the range of 0.20 and 0.70. The results of force tests and hinge-moment measurements were presented in reference 1. This report presents the results of chordwise and spanwise pressure-distribution measurements.

In the application of wind-tunnel data obtained with solid models of exact profile contour to the calculation of aerodynamic loads on a full-scale airplane wing or tail, it is difficult to allow for the effects of surface distortion. Because surface distortion ordinarily increases with increasing speed and because the effects of a given surface irregularity become magnified at high Mach number, high-speed full-scale tests of actual components of high-speed airplanes are required to determine accurately the aerodynamic characteristics and to investigate the nature of the effects of structural distortion.

The purpose of the present investigation was to supplement the force tests of reference 1 with pressure data which would provide detailed information as to the nature of the flow changes with increasing speed.

The tail surface used in this investigation is considered to be typical of present practice as regards structural characteristics, and the results obtained should therefore be generally applicable to the design of tail surfaces for fighter-type airplanes.

SYMBOLS

c_{n_α} section normal-force parameter $\left(\dfrac{\partial c_n}{\partial \alpha}\right)$

$c_{n_{\delta_e}}$ section normal-force parameter $\left(\dfrac{\partial c_n}{\partial \delta_e}\right)$

c_n section normal-force coefficient

C_{bm} root-bending-moment coefficient $\left(\dfrac{1}{c_s b^2}\right)\displaystyle\int_0^{b/2}\left(c c_n\right)y\ dy$

P pressure coefficient $\left(\dfrac{p - p_0}{q_0}\right)$

P_α rate of change of pressure coefficient with angle of attack

P_{δ_e} rate of change of pressure coefficient with elevator angle

P_{R_α} rate of change of resultant pressure coefficient with angle
        of attack (resultant pressure coefficient = $P_{lower} - P_{upper}$)

M_{cr} critical Mach number (air-stream Mach number at which local velocity first equals velocity of sound of stream)

p   static pressure at any point

q   dynamic pressure $\left(\frac{1}{2}\rho V^2\right)$

b   span of model (90 in.)

c_s root chord (50 in.)

c   chord at any spanwise station   y,   inches

y   distance from root chord to any station, inches

x   distance from leading edge

c_e elevator chord aft of hinge line

α   stabilizer angle of attack, degrees

δ_e angle of elevator chord with respect to stabilizer chord (trailing edge down is positive), degrees

Subscripts:

e   elevator

o   free stream

t   trim tab

APPARATUS AND METHODS

A full-scale horizontal tail surface was tested in the Langley 16-foot high-speed tunnel. (See fig. 1.) The tail surface was constructed by present-day production methods and was of metal construction, metal covered, and flush riveted. A 10-percent-thick symmetrical airfoil was used and the ordinates are presented in table I. The variation of the actual tail-surface contour from the specified contour is illustrated in figure 2. The tail surface had an aspect ratio of 4.65, a taper ratio of 0.56, and 5° dihedral. The elevator was of the sealed internally balanced type and had a straight contour aft of hinge line (70 percent chord) resulting in a trailing-edge angle of approximately 14°. (See fig. 3.) The elevator balance chamber was housed in the stabilizer and is shown in detail in figure 4. The flow of air through the elevator gap from the high-pressure to low-pressure side of the tail surface was prevented by

a rubber-covered fabric seal which extended between the nose of the balance plate and the balance chamber and around the hinge pocket.

The model was constructed with orifices at three spanwise stations for measuring external pressures and at four stations in the balance chamber. Heavy-walled $\frac{1}{8}$-inch-diameter copper tubing was used for the orifices which resulted in an orifice diameter of approximately 0.050 inch. The orifices were not located on ribs and the data obtained with them include effects of skin distortion. The location of the orifices with respect to ribs and stringers is shown in figure 5. All pressures were recorded simultaneously by photographing multitube manometers

TESTS

Data were obtained for angles of attack of $-3°$, $-1\frac{1}{2}°$, $0°$, $1\frac{1}{2}°$, $3°$, and $6°$; elevator angles of $-17°$, $-13°$, $-9°$, $-6°$, $-4°$, $-2°$, $0°$, $2°$, $4°$, $6°$, and $9°$; and Mach numbers of 0.20, 0.30, 0.40, 0.50, 0.55, 0.60, 0.65, and 0.68. Any combination of these variables was limited by the maximum allowable load on either the stabilizer, elevator, or tail surface as a unit, the allowable load being taken as three-fourths of the design limit load. The average dynamic pressures and average Reynolds numbers corresponding to the test Mach numbers are shown in figure 6. The Reynolds number is based on the mean aerodynamic chord of 40 inches. All data presented in this report were obtained with the trim tab in its neutral position.

REDUCTION OF DATA

The pressure measurements were reduced to the usual coefficient form $P = \dfrac{p - p_0}{q_0}$. The rates of change of pressure coefficient with angle of attack and elevator angle were obtained by plotting the pressure at each orifice against angle of attack and elevator angle and measuring the slope over the linear portion of the lines. Since structural considerations limited the combinations of angle of attack and elevator angle that could be tested above $M = 0.60$ and thus prevented the accurate determination of slope data, no slope data are presented above $M = 0.60$.

The section normal-force coefficients were obtained by mechanical integration of the chordwise pressure-distribution plots. These

values of section normal—force coefficients were then plotted
against angle of attack and also elevator angle and the slope of the
curves measured. c_{n_α} and c_{n_δ} could also be obtained with fair
accuracy by mechanical integration of the chordwise plots of P_α
and P_{δ_e}.

The angle of attack of the tail surface has been corrected for
wind—tunnel wall interference by the method of reference 2. Applica-
cation of the method of reference 3 for blockage corrections indicated
that the maximum correction to dynamic pressure was less than 1 per-
cent for the range of test of the subject model and therefore no
blockage corrections are included.

RESULTS AND DISCUSSION

Chordwise distributions.— The basic pressure distribution for
the zero angle of attack and elevator angle at Mach numbers of 0.20,
0.40, and 0.60 are presented in figures 7, 8, and 9 for the 18—inch,
47.5—inch, and 81—inch stations, respectively. The effect of the
surface irregularities on the pressure distribution is apparent when
figure 8 is used in conjunction with figure 2. It is indicated that
the surface irregularities had an appreciable adverse effect on the
pressure distribution and as will be discussed later, lowered the
critical Mach number of the tail surface. The agreement between the
location of the surface irregularities and the distortions of the
pressure distribution is reasonably good, although in some cases
lack of sufficient pressure orifices makes the actual shape of the
pressure diagram somewhat doubtful.

The chordwise variations of the rate of change of pressure
coefficient with angle of attack are presented in figure 10 for the
18—inch, 47.5—inch, and 81—inch stations at $M = 0.20$, 0.40, and 0.60.
This figure shows an increase in P_α over the leading 60 percent of
the airfoil as the Mach number is increased, due to compressibility
effects, while no systematic variation was apparent aft of the hinge
line. The pressure distribution at any angle of attack or fraction
thereof from $\alpha = -3^\circ$ to 3° can be obtained by multiplying the slope
data by the desired angle and then adding the values of pressure
coefficient for the zero angle of attack. (See figs. 7 to 9.) The
dashed parts of the P_α curves represent pressures which change very
rapidly due to movement of the stagnation point or elevator protrusions,
and for which appreciable error in determining the slopes is possible.

The chordwise distribution of the rate of change of pressure
coefficient with elevator angle P_{δ_e} at the 18—inch, 47.5—inch,

and 81-inch stations for Mach numbers of 0.20, 0.40, and 0.60 is
shown in figure 11. This figure shows a decrease in P_{δ_e} with
increasing Mach number over the leading 15 percent of tail surface
and an increase at 70 and 77 percent of the chord. The decrease
of P_{δ_e} at the leading edge with increasing Mach number is contrary
to data obtained from solid models of high torsional rigidity and
appears to be caused by twist of the stabilizer in a direction to
decrease the lift due to the center of pressure moving rearward as
the elevator angle is increased. It is estimated that a decrease
of approximately 0.10 of a degree in angle of attack would account
for the reduction in P_{δ_e} between $M = 0.2$ and $M = 0.6$ shown in
figure 11.

The effect of Mach number on the chordwise pressure distribution
for constant c_n was investigated. However, no data are shown
because the effect was negligible and no appreciable shift in the
center of pressure was indicated between a Mach number of 0.20 and 0.60.

Since the data for the rate of change of pressure coefficient
with angle of attack or elevator angle are applicable only for a
limited range of angles $(\alpha = \pm 3^\circ, \delta_e \pm 8^\circ)$, the chordwise pressure
distributions for a few larger angles of attack and elevator deflec-
tion are presented in figures 12 to 16 for the 18-inch, 47.5-inch,
and 81-inch stations at $M = 0.20$.

Figure 17 presentes the percent change with Mach number in
hinge-moment coefficient and elevator-balance pressure coefficient for
several combinations of angle of attack and elevator angle. An
increase in the absolute value of either coefficient between $M = 0.20$
and any other Mach number has been considered positive and a decrease,
negative. This figure shows that the hinge-moment coefficient
increases more than the balance-chamber pressure coefficient decreases
as the speed is increased. Thus only a part of the increase in
hinge-moment coefficient with increasing speed can be attributed to a
loss of balance chamber pressure. Figures 11 and 18 show that in
general the elevator pressures increase with increasing Mach number
particularly between 0.7 and 0.8 chord. These increases also
contribute to the rise in hinge-moment coefficients with Mach number.
The combined effects of the pressure changes shown in figures 17
and 18 indicate changes in hinge-moment coefficients which are in
approximate agreement with the force-test results.

Spanwise distribution.- The variation of spanwise distribution
of the section normal-force coefficient as obtained from the tests
and as calculated according to reference 4 is shown in figure 19.

No unusual loading conditions are apparent for the speeds tested and the agreement between the calculated and experimental data is reasonably good.

Effect of Mach number on root-bending moment.- The variation of the root-bending-moment coefficient with Mach number is shown in figure 20 for the calculated and experimentally determined span loadings. When the normal force was obtained by deflecting the elevator, the root bending moment decreased slightly at the higher speeds, whereas when the normal force was obtained by changing the angle of attack the root-bending moment increased slightly. However, no significant difference between the calculated and experimental root-bending-moment coefficients was apparent up to a Mach number of 0.68.

Estimated critical Mach numbers.- Extrapolation of the experimental pressure data by the Temple-Yarwood method indicated that this tail surface would have a critical Mach number of 0.77 at $C_L = 0$ and $\delta = 0^O$. However, from consideration of the effects of the peaks in the pressure diagrams and the calculated pressure distribution for a smooth airfoil it is estimated that the critical Mach number could be increased to 0.80 if the airfoil surface were ideally smooth and fair. (See reference 5.) The variation of the critical Mach number with angle of attack for various elevator angles is shown in figure 21.

It should be emphasized that except for the determination of the critical Mach number the data and trends which have been discussed cannot be safely extrapolated to higher speeds because of the radical changes which occur at speeds above the critical speed.

CONCLUSIONS

1. Lack of fairness of the surface had an appreciable adverse effect on the pressure distribution which adversely affects the M_{cr} over the airfoil. The highest critical speed of the tail surface was 0.77; however, it is estimated that this could be increased to 0.80 by eliminating the surface irregularities.

2. The rate of change of pressure coefficient with angle of attack over the leading 60 percent of the chord increased with increasing Mach number due to compressibility effects, while no systematic variation was apparent aft of the hinge line.

3. The rate of change of pressure coefficient with elevator angle decreased over the leading 15 percent of the tail surface as

a result of model twist and increased at the 70-percent and 77-percent chord stations with increasing Mach number.

4. The increase in hinge-moment coefficient with increasing speed was found to result from a loss of pressure in the elevator balance chamber and an increase in the external elevator pressures aft of the hinge line.

5. Reasonable agreement between the calculated and experimental root-bending-moment coefficient was obtained up to a Mach number of 0.68.

Langley Memorial Aeronautical Laboratory
    National Advisory Committee for Aeronautics
        Langley Field, Va.

REFERENCES

1. Schueller, Carl F., Hieser, Gerald, and Cooper, Morton: Aerodynamic Force Characteristics at High Speeds of a Full-Scale Horizontal Tail Surface Tested in the Langley 16-Foot High-Speed Tunnel. NACA RM No. L7D08a, 1947.

2. Swanson, Robert S., and Toll, Thomas A.: Jet-Boundary Corrections for Reflection-Plane Models in Rectangular Wind Tunnels. NACA ARR No. 3E22, 1943.

3. Thom, A.: Blockage Corrections in a Closed High-Speed Tunnel. R. & M. No. 2033, British A.R.C., 1943.

4. Anon.: Spanwise Air-Load Distribution. ANC-1 (1), Army-Navy-Commerce Committee on Aircraft Requirements. U.S. Govt. Printing Office, April 1938.

5. Robinson, Harold L.: High-Speed Investigation of Skin Wrinkles on Two NACA Airfoils. NACA TN No. 1121, 1946.

TABLE I

SECTION PROPERTIES OF THE AIRFOIL TESTED

SYMMETRICAL SECTION

Percent x	Percent y
0	0
.5	.788
.75	.964
1.25	1.24
2.5	1.74
5	2.421
7.5	2.915
10	3.307
15	3.903
20	4.330
25	4.635
30	4.841
35	4.961
40	5
45	4.9603
50	4.8387
55	4.6347
60	4.347
65	3.979
70	3.5363
75	3.0274
80	2.4634
85	1.8595
90	1.233
95	.6052
100	0

NATIONAL ADVISORY
COMMITTEE FOR AERONAUTICS
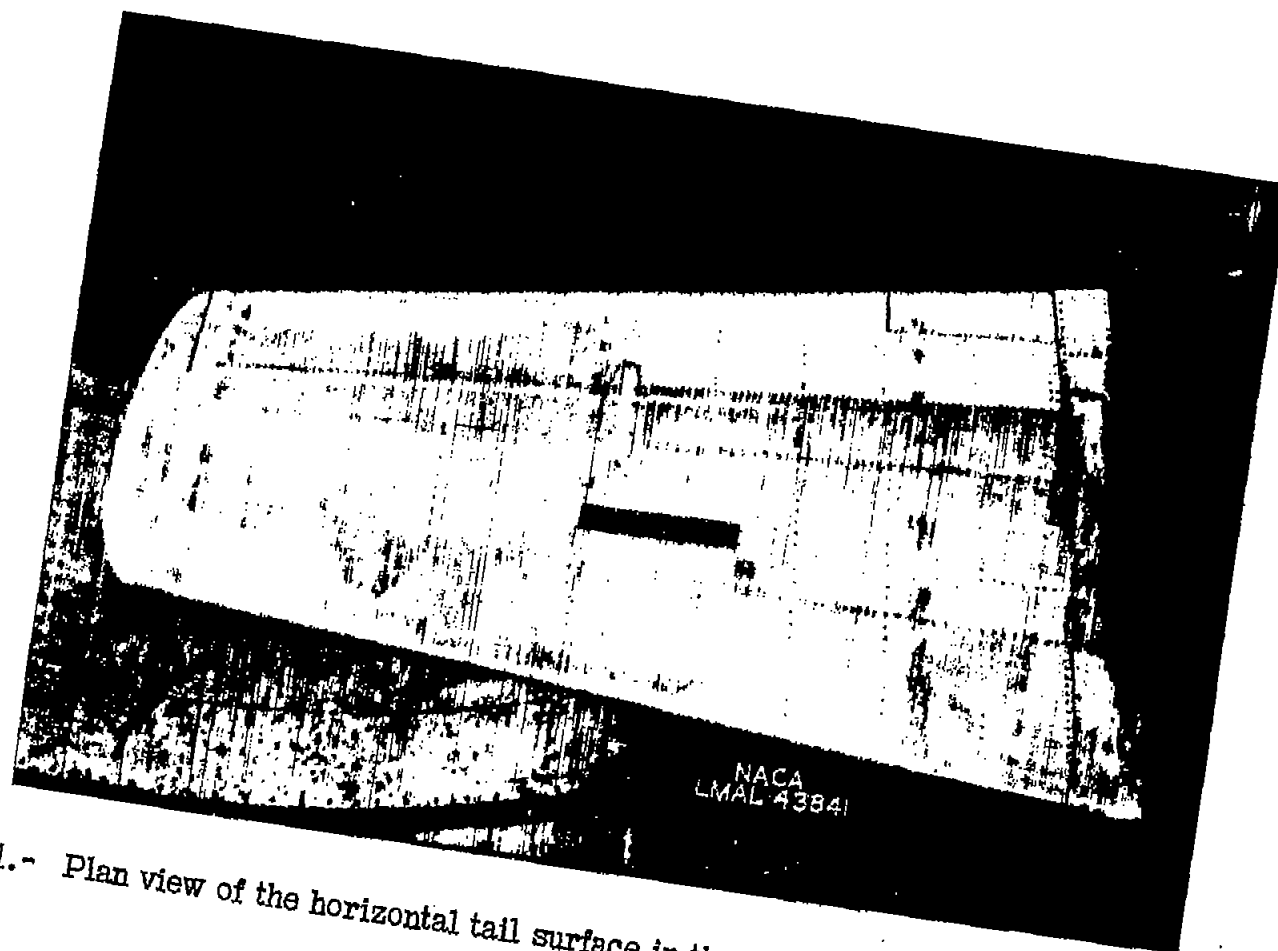
Figure 1.- Plan view of the horizontal tail surface in the Langley 16-foot high-speed tunnel.

Fig. 1
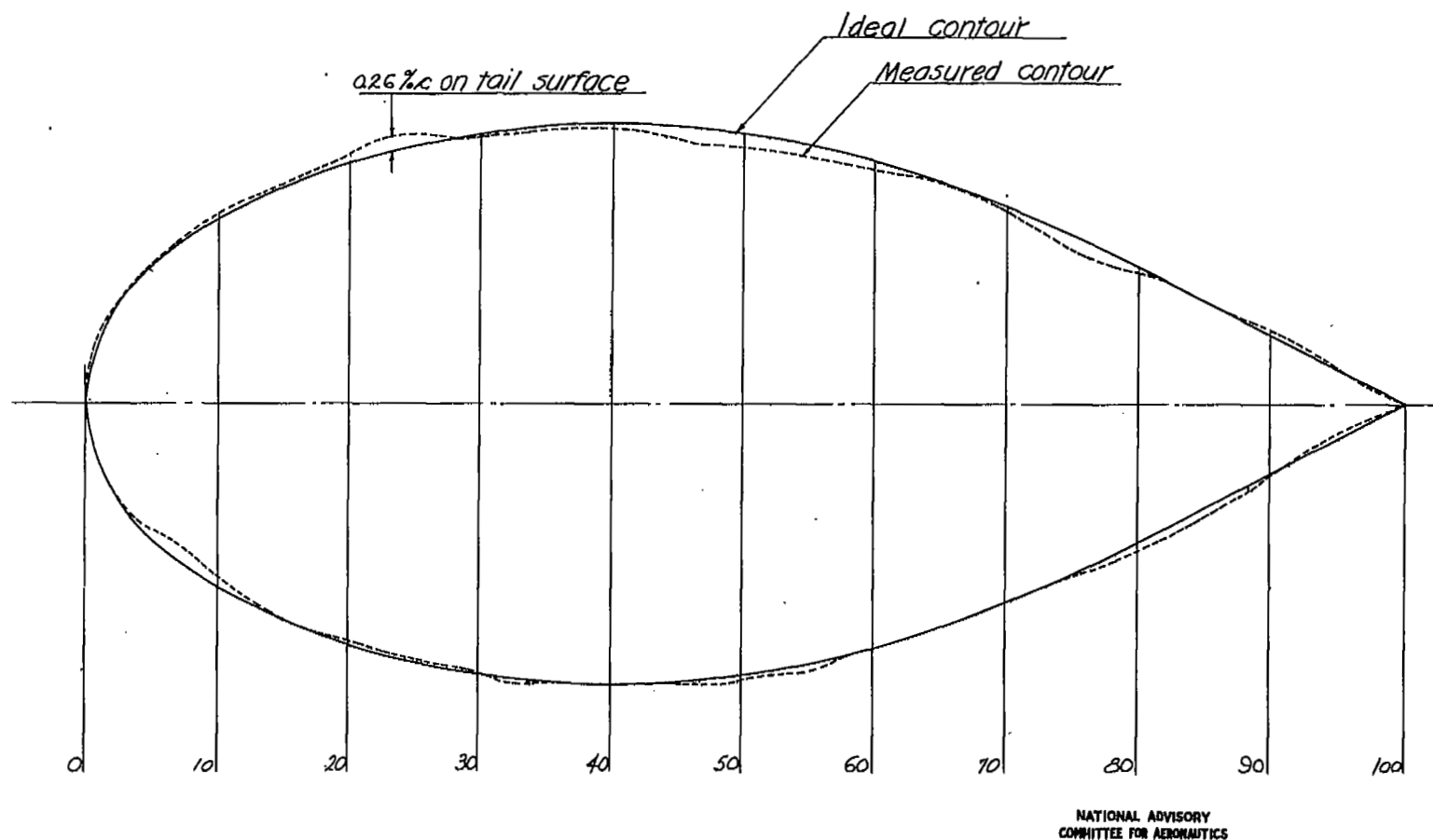
Figure 2 .——Comparison of the measured and ideal contour of the tail surface at the 47-inch station. (Thickness increased four times.)

Fig. 2

Fig. 3

Republic R-4-40-010 Airfoil section
Dihedral of tail = 5°
Elevator trailing-edge angle ≈ 14°
All dimensions in inches

NATIONAL ADVISORY
COMMITTEE FOR AERONAUTICS

Figure 3.— General arrangement of the horizontal tail surface.
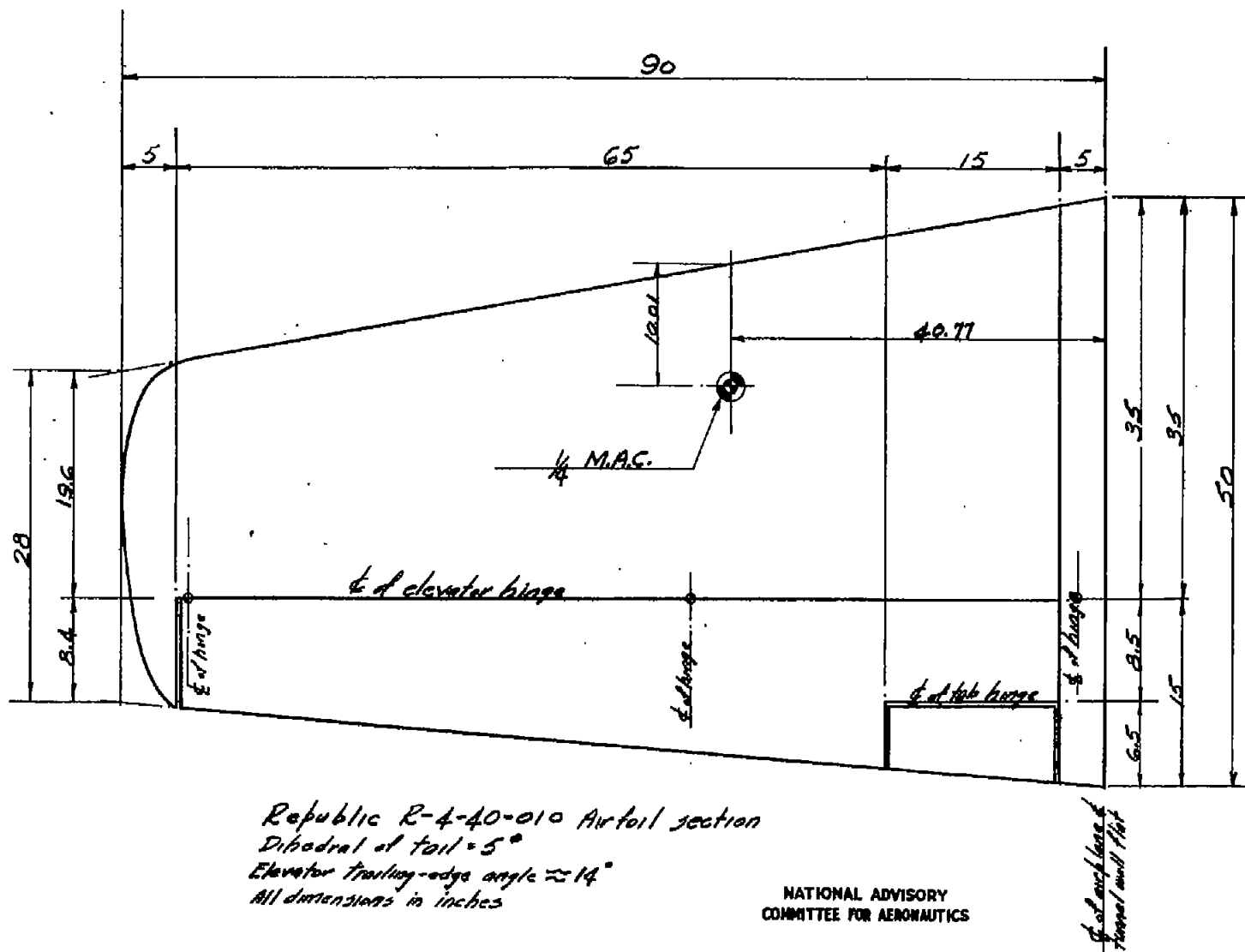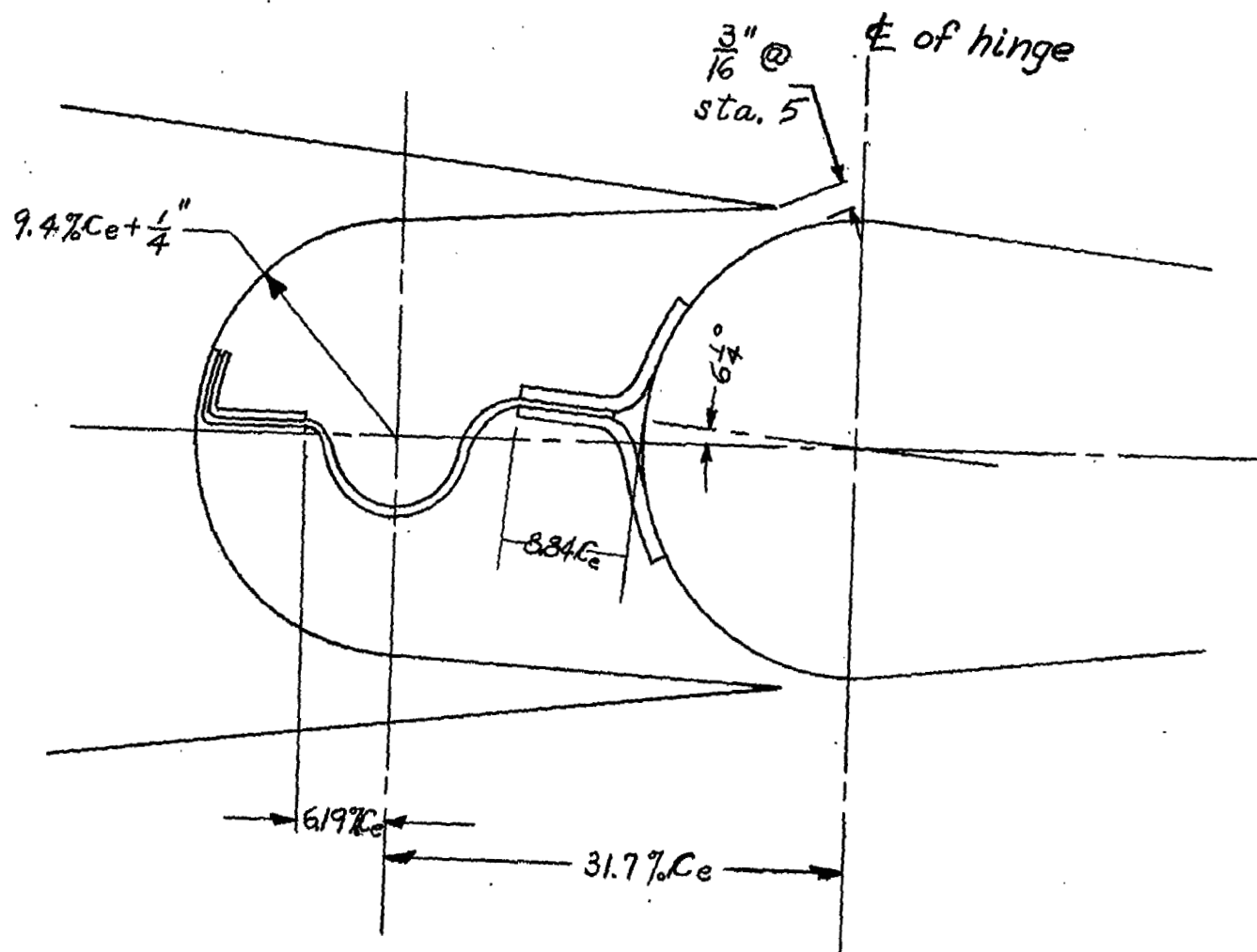
Figure 4. - Detail of balance chamber.

Fig. 4
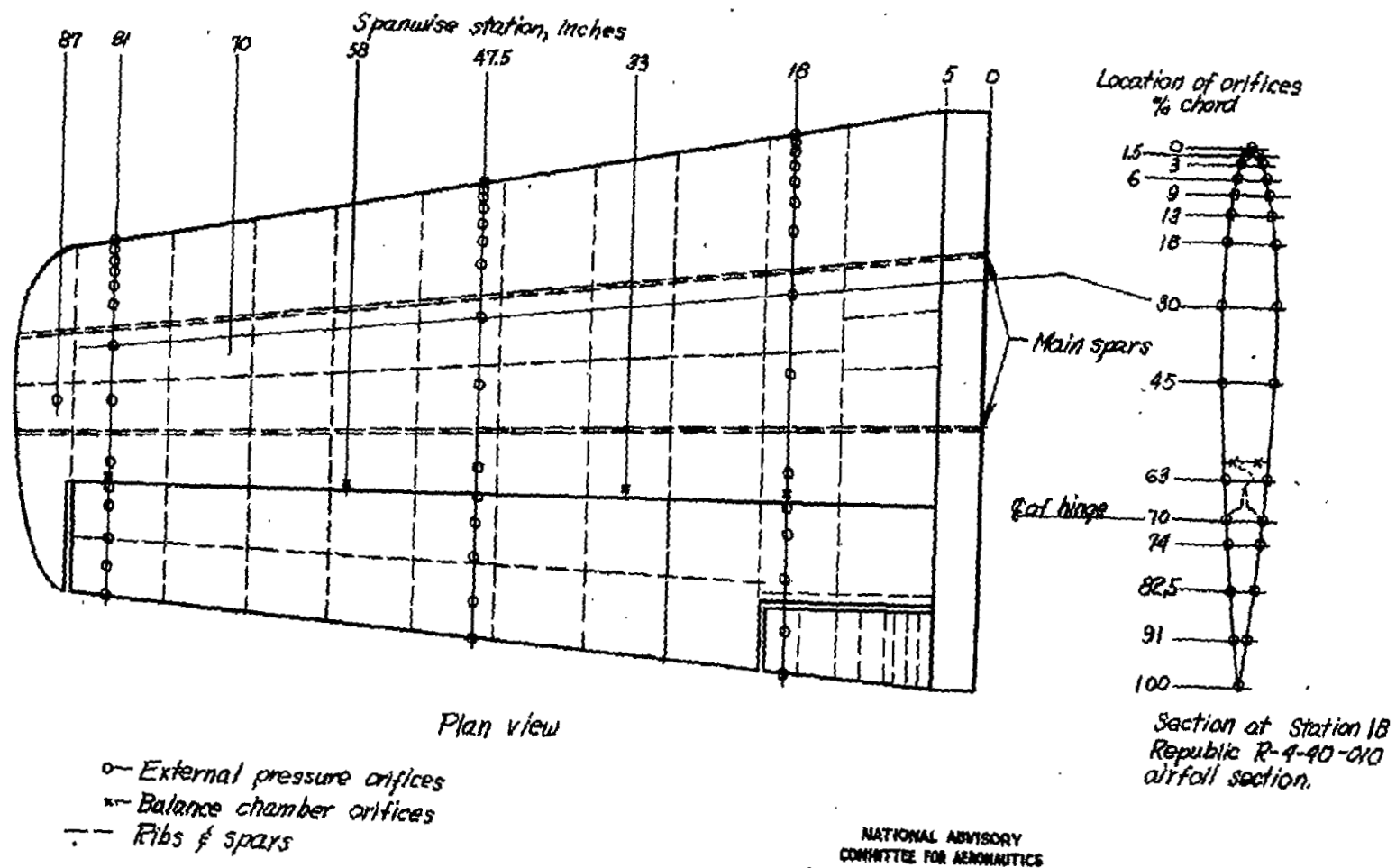
Figure 5. — Orifice locations on the horizontal tail surface.

Fig. 5

Figure 6.— Variation of the average test Reynolds number and dynamic pressure with test Mach number.
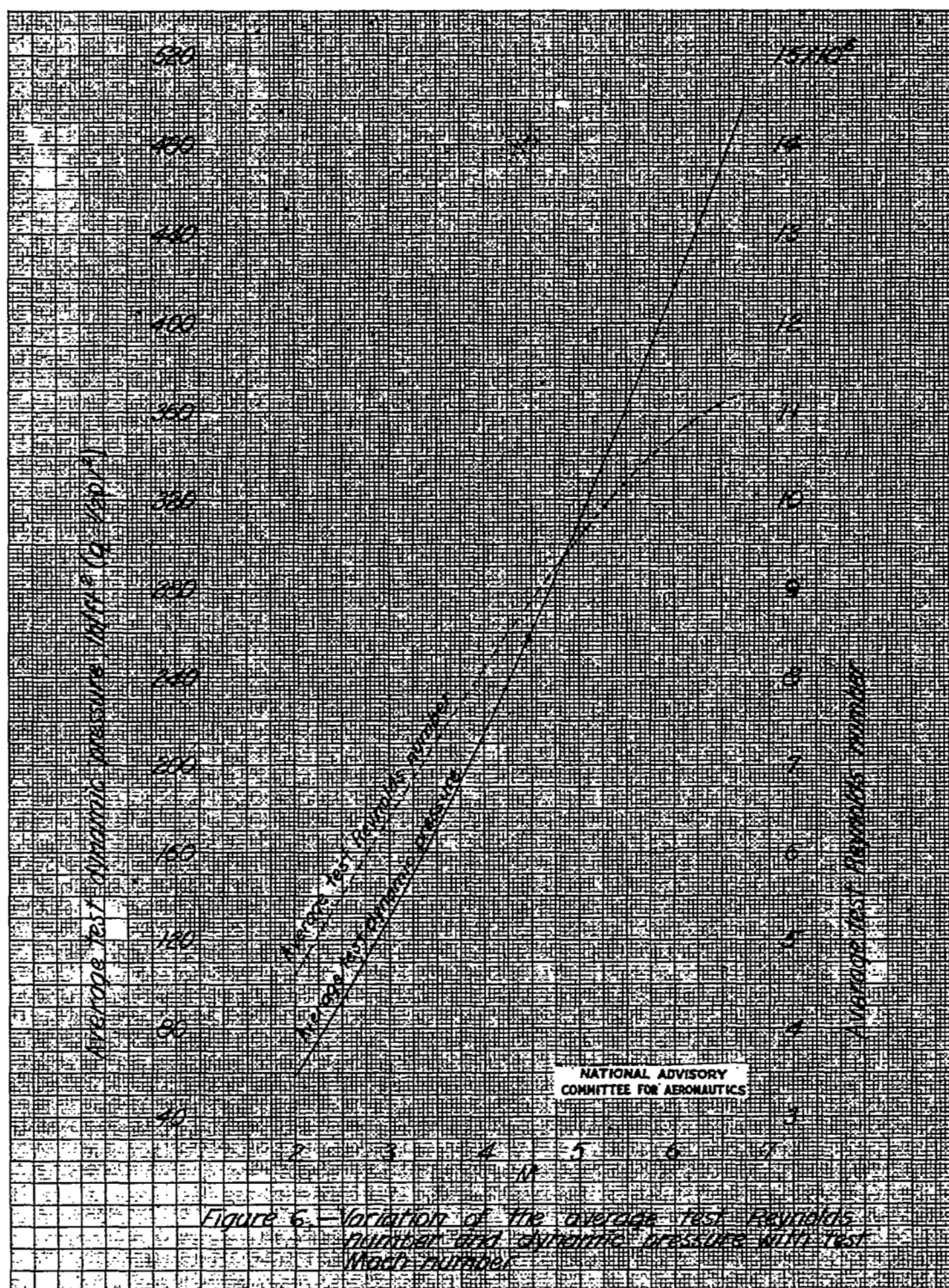
Fig. 7   NACA RM No. L7D08
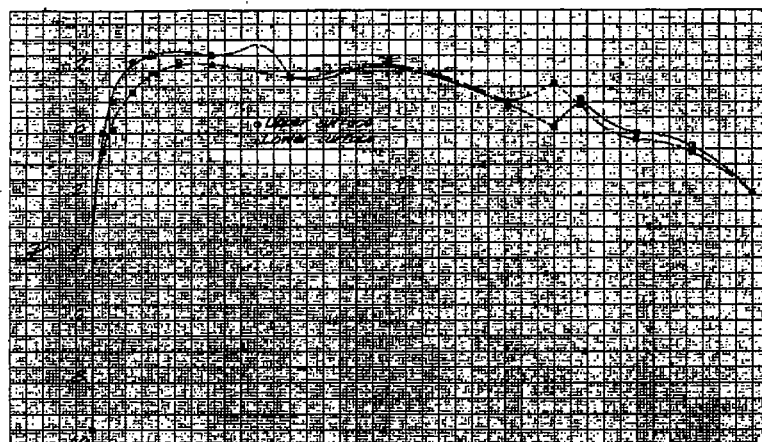
(a) M=0.20
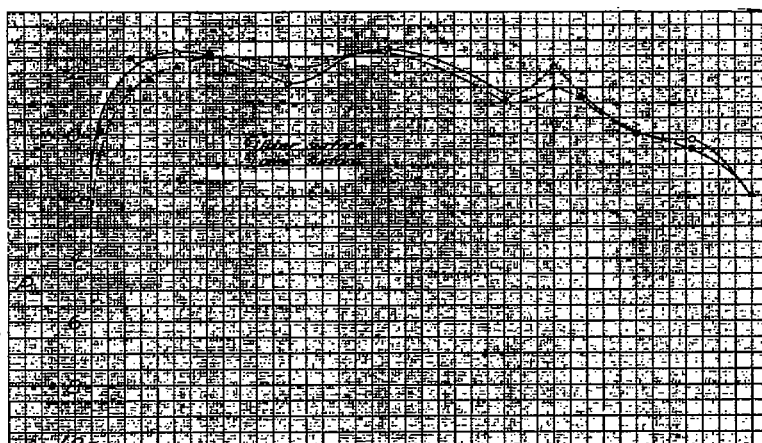
(b) M=0.40
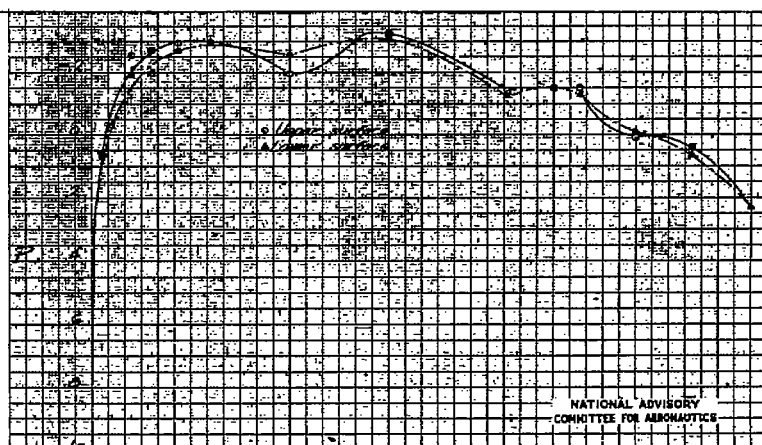
(c) M=0.60

0   .1   .2   .3   .4   .5   .6   .7   .8   .9   1.0
                              x/c

Figure 7 .— Pressure distribution at the 18-inch station, α=0°, δ_e=0°, δ_r=0°.
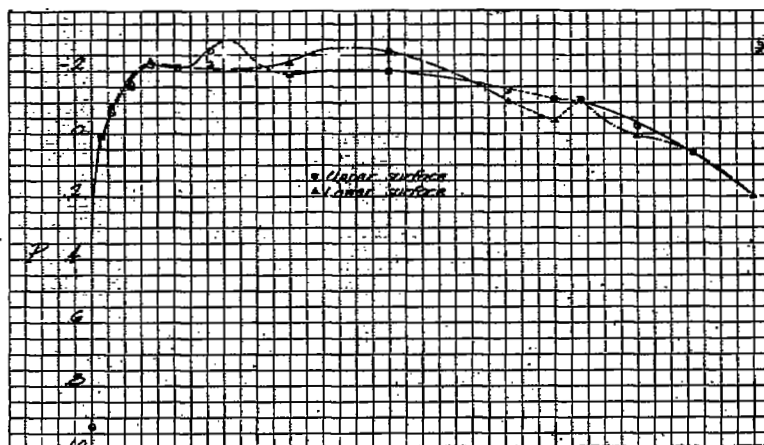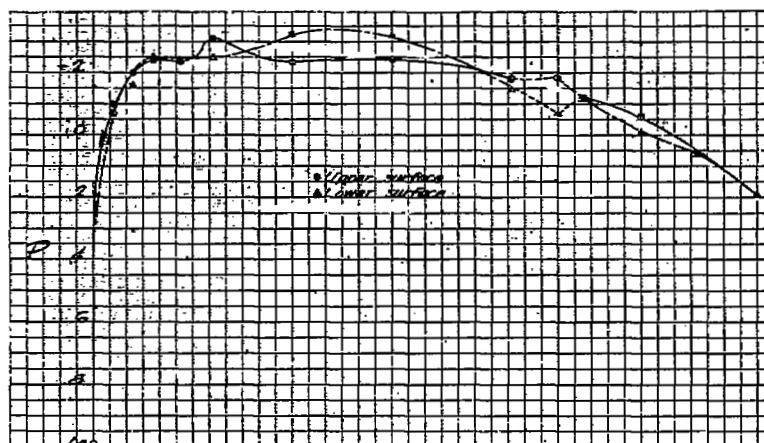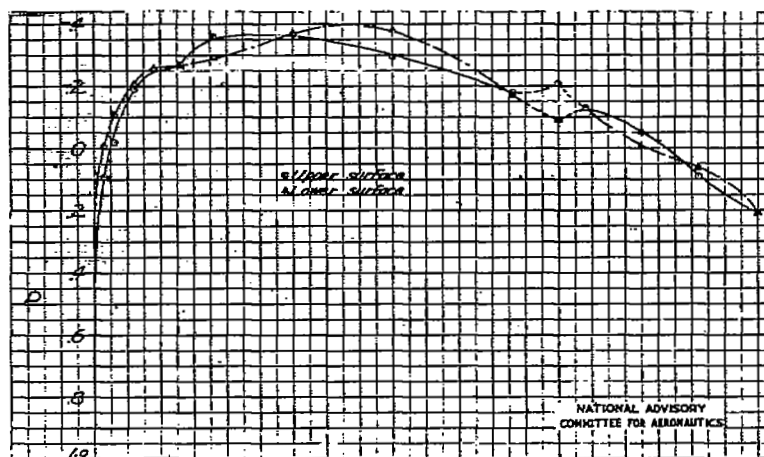
(a) M=0.20

(b) M=0.40

(c) M=0.60

Figure 8 .— Pressure distribution at the 47.5-inch station, $\alpha=0°$, $d_e=0°$, $d_f=0°$.

Fig. 9

(a) M=0.20

(b) M=0.40

NATIONAL ADVISORY
COMMITTEE FOR AERONAUTICS
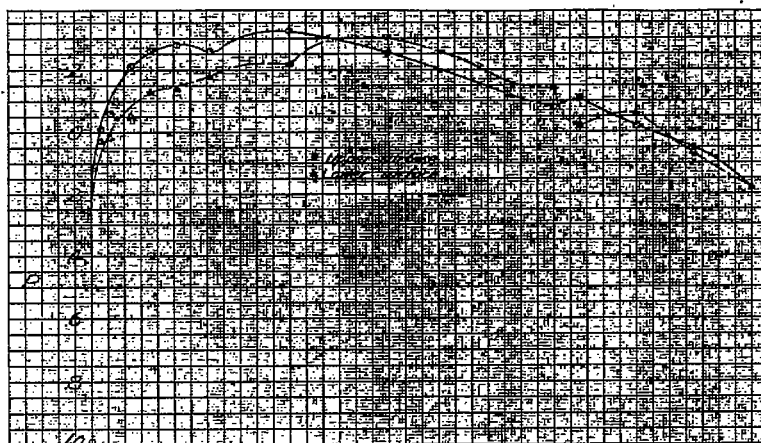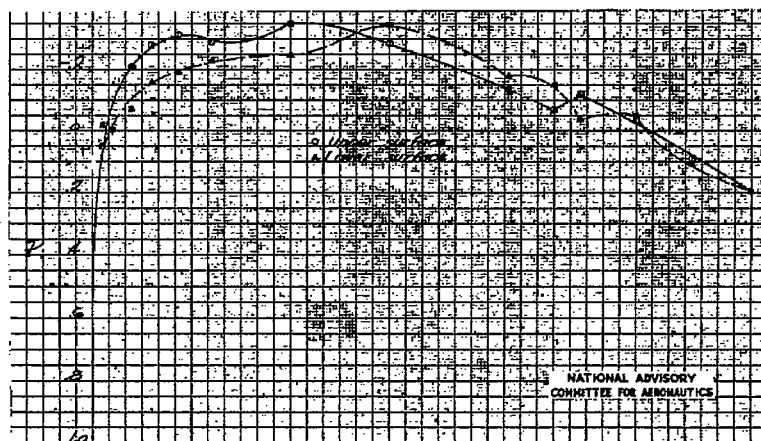
(c) M=0.60

0   .1   .2   .3   .4   .5   .6   .7   .8   .9   1.0
                              x/c

Figure 9 — Pressure distribution at the 61-inch station, $\alpha = 0°$, $\delta_e = 0°$, $\delta_f = 0°$.
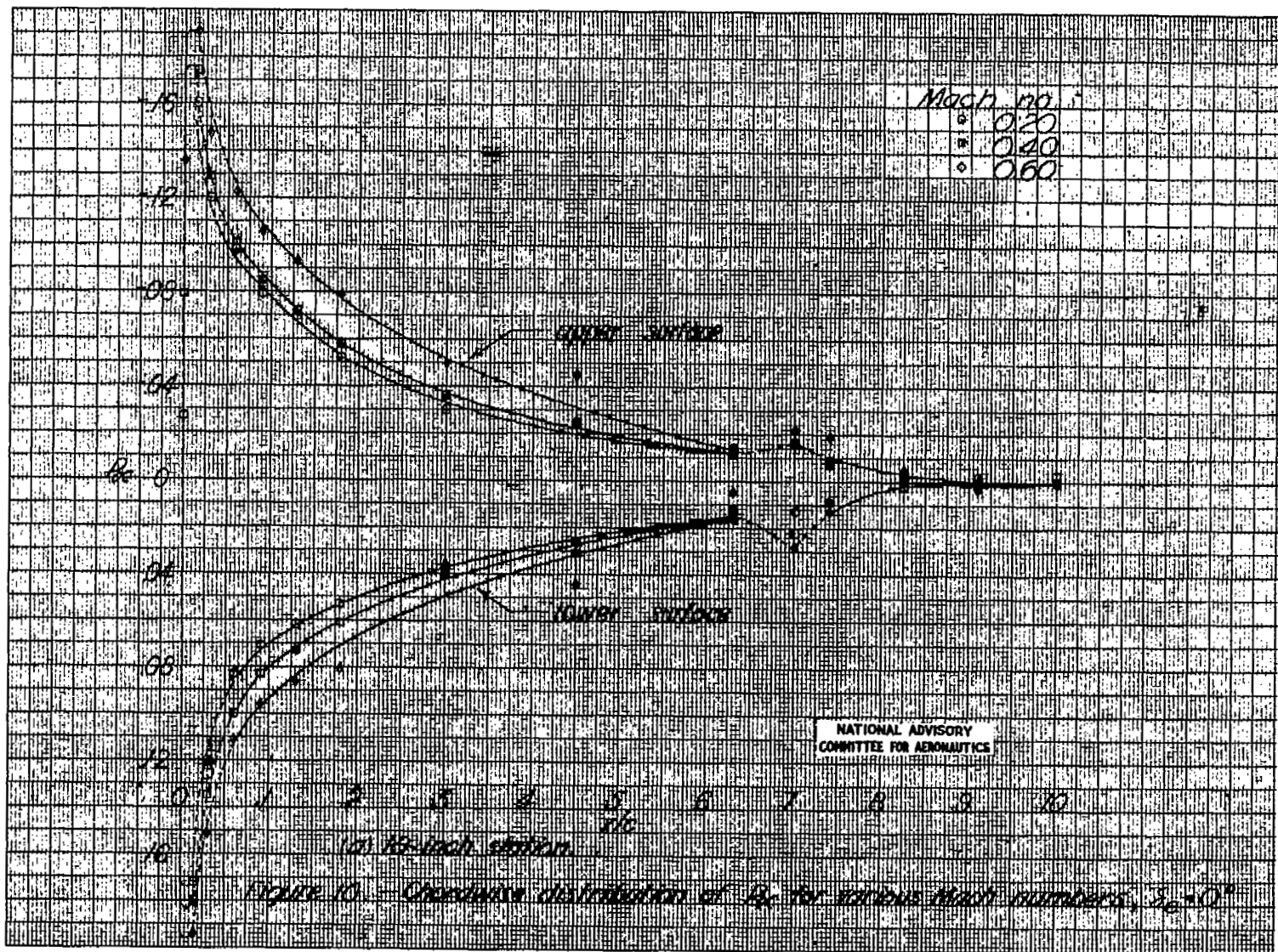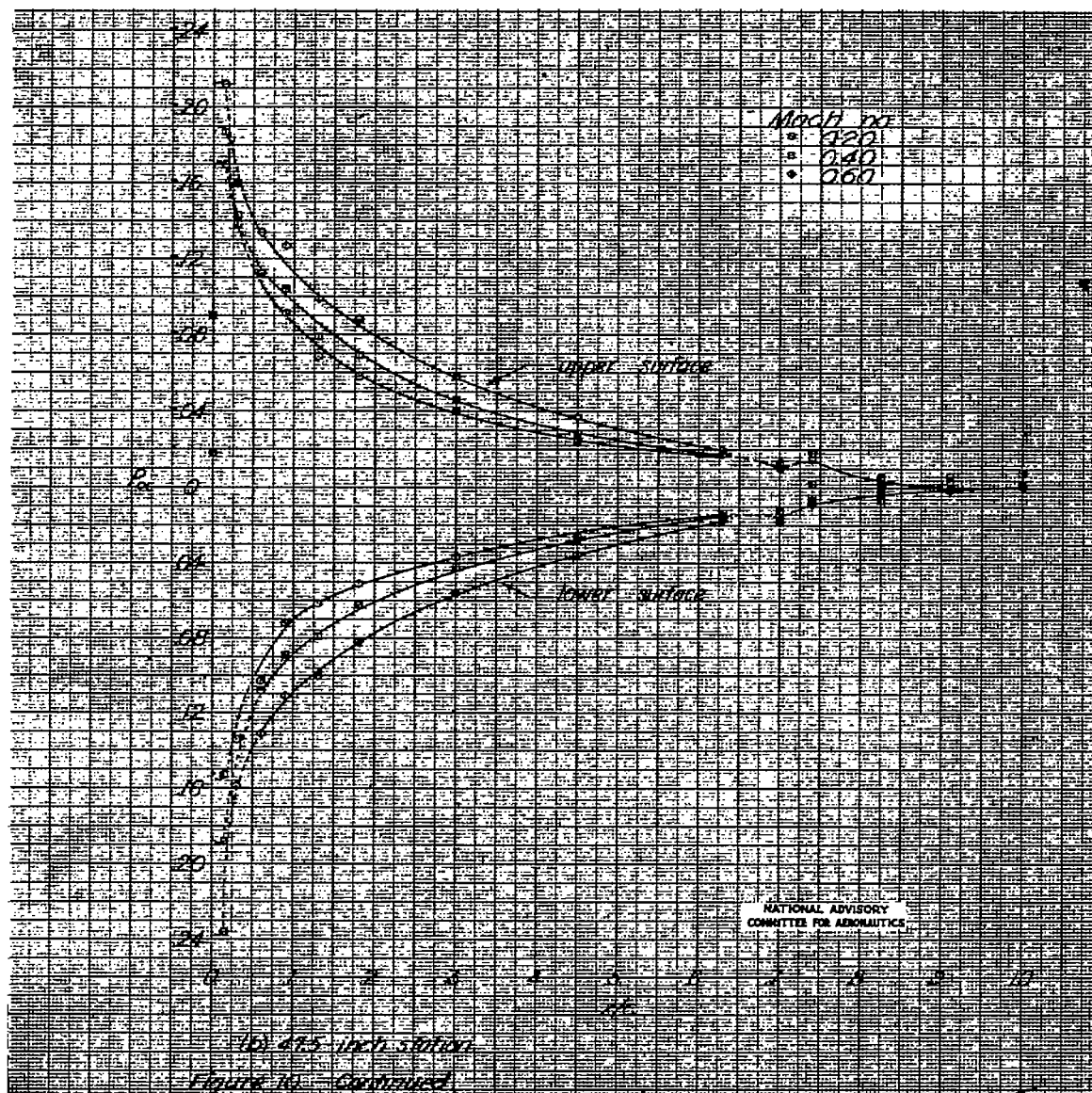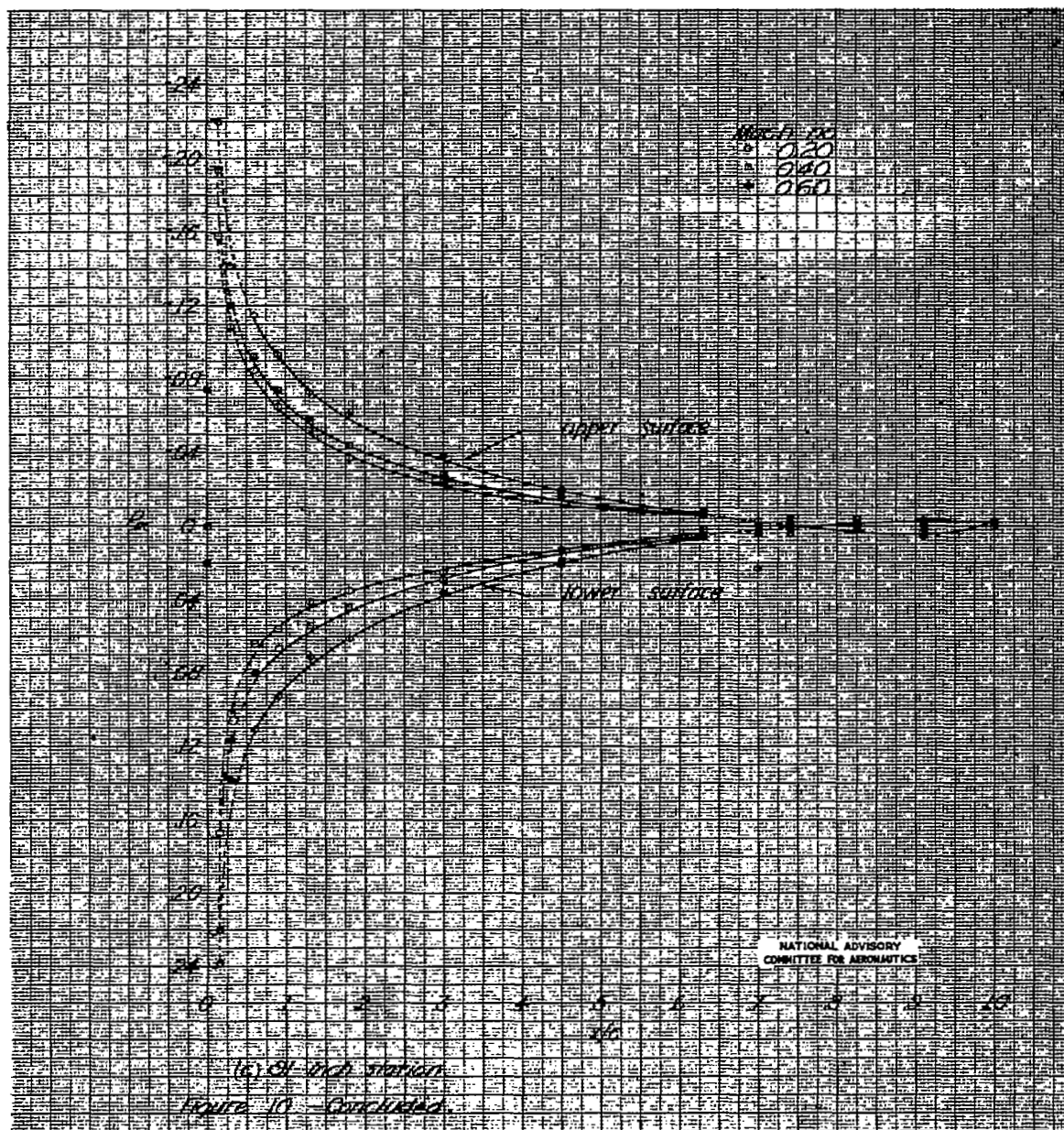
(a) Inboard station.

Figure 10.- Chordwise distribution of P_c for various Mach numbers. $\delta_e = 0°$

(b) 47.5 inch station.

Figure 10.- Continued.

(c) 31-inch station.

Figure 10.- Concluded.

(a) 13-inch station.

Figure 11.— Chordwise distribution of P_R for various Mach numbers; $\alpha = 0°$.

NATIONAL ADVISORY
COMMITTEE FOR AERONAUTICS

(b) 41.5 inch station.

Figure 11. - Continued.
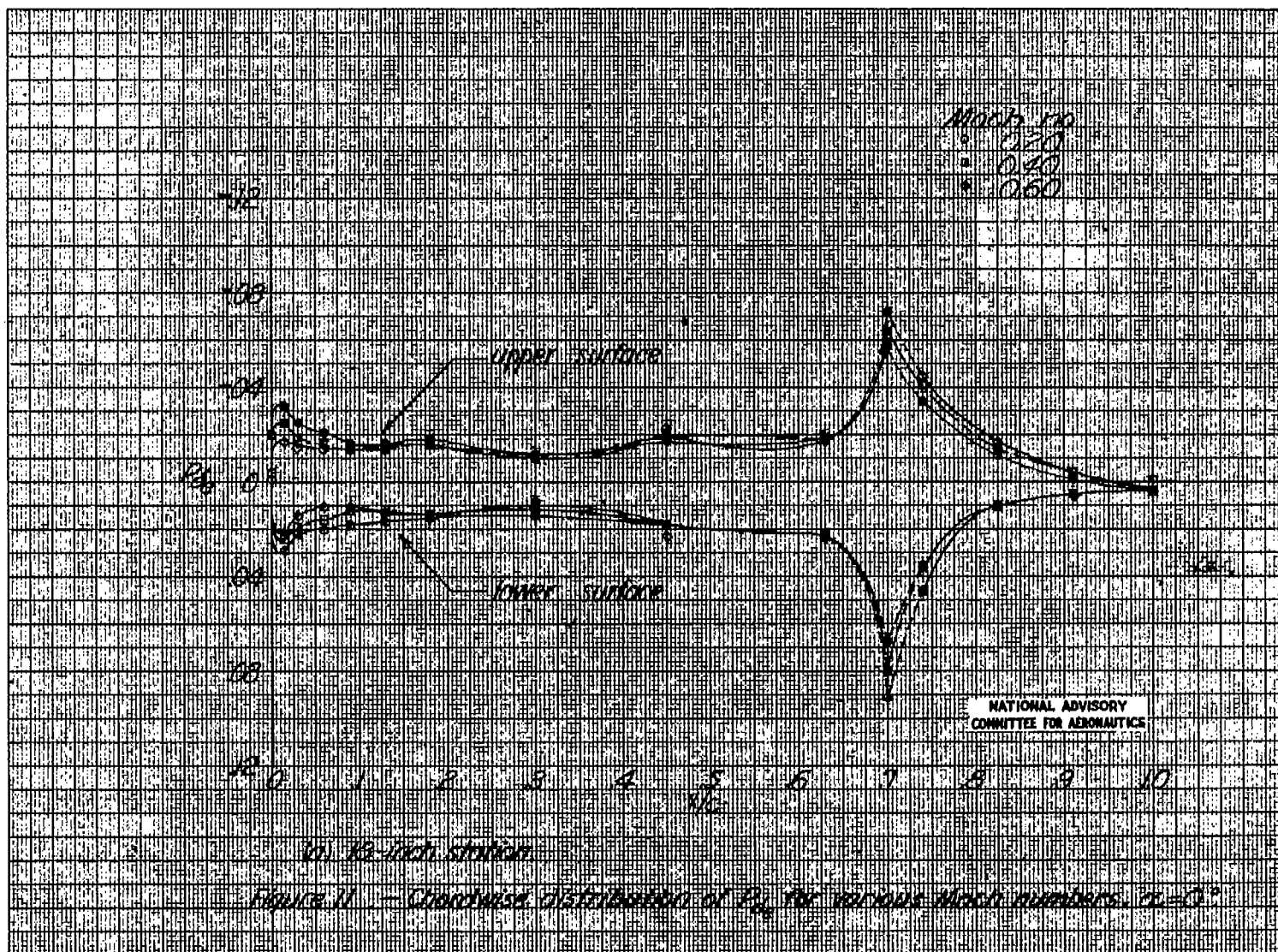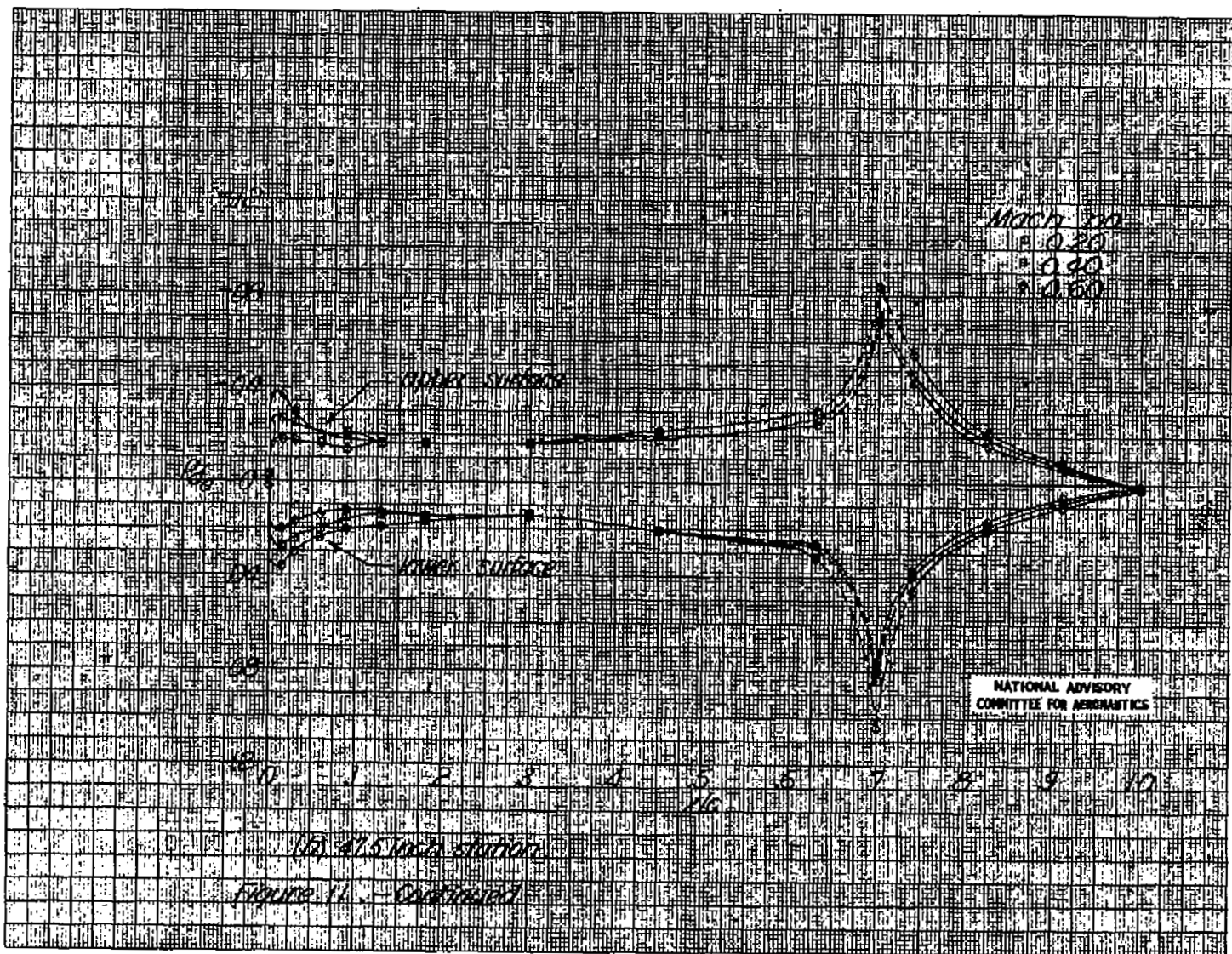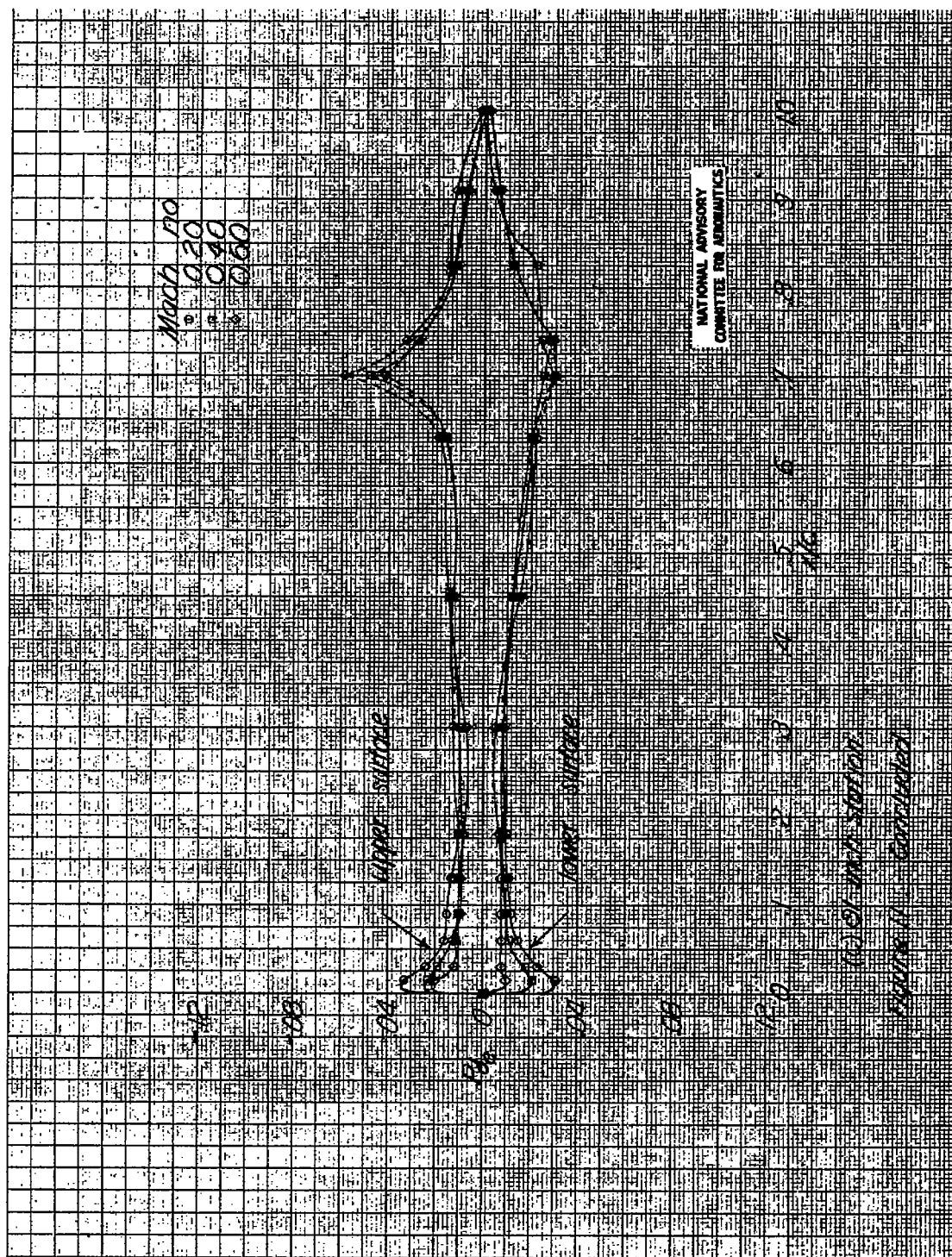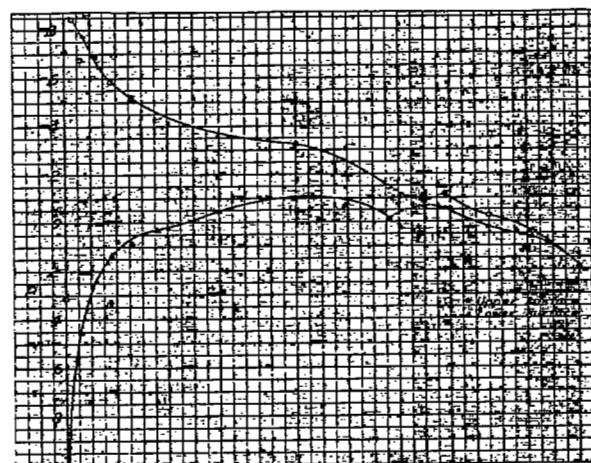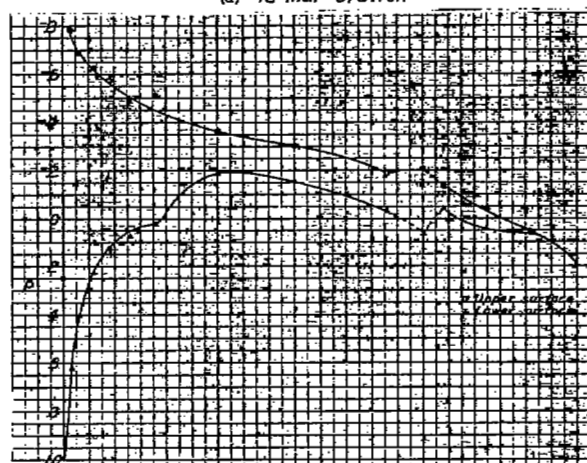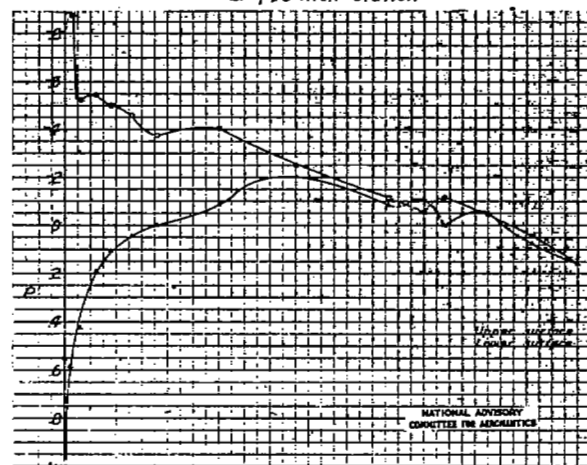
(a) 18-inch station

(b) 47.5-inch station

(c) 81-inch station

Figure 12.—Pressure distribution at M=0.20 for $\delta_e=0°$; $\delta_r=0°$; $\alpha=4.3°$.

Fig. 13   NACA RM No. L7D08
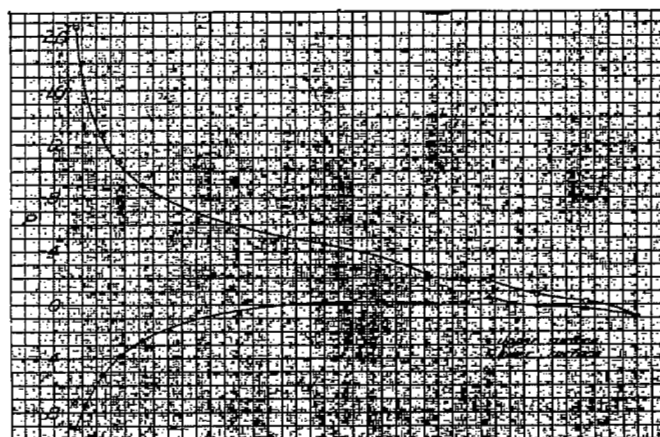
(a) 18-inch station
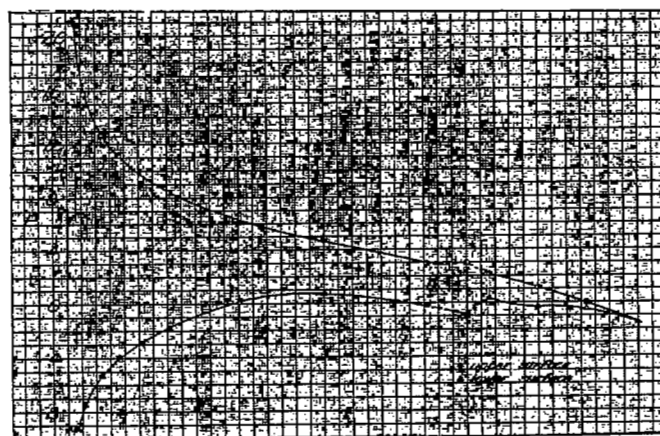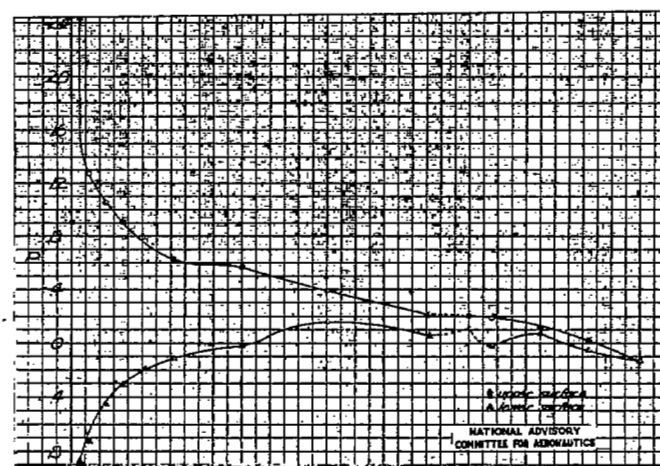
(b) 47.5-inch station

(c) 81-inch station

Figure 13 .—Pressure distribution at M=0.20 for δ_e=-0.1°; δ_b=0°; $\propto$ = 8.6°.

(a) 18-inch station

(b) 47.5-inch station

NATIONAL ADVISORY
COMMITTEE FOR AERONAUTICS
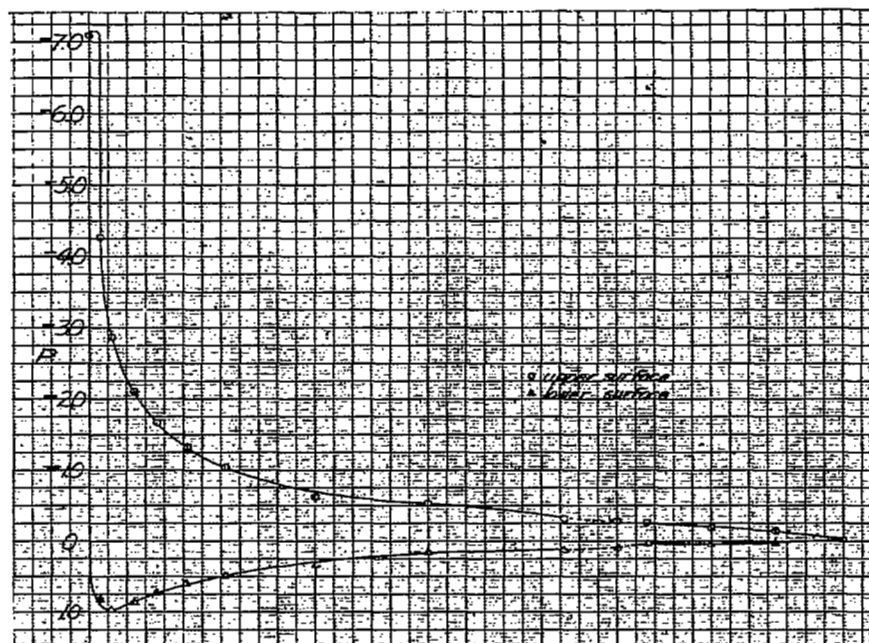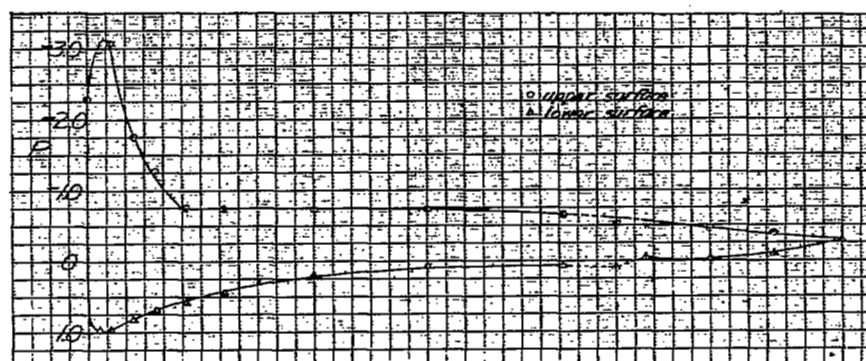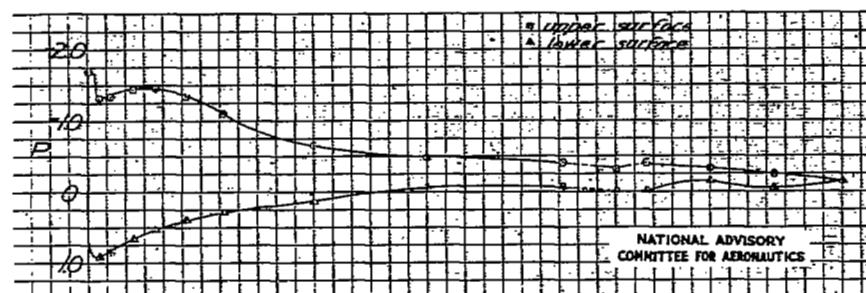
(c) 81-inch station

Figure 14.- Pressure distribution at M=0.20 for δ_e=-0.3°; δ_b=0°; α=17.0°.

Fig. 15   NACA RM No. L7D08
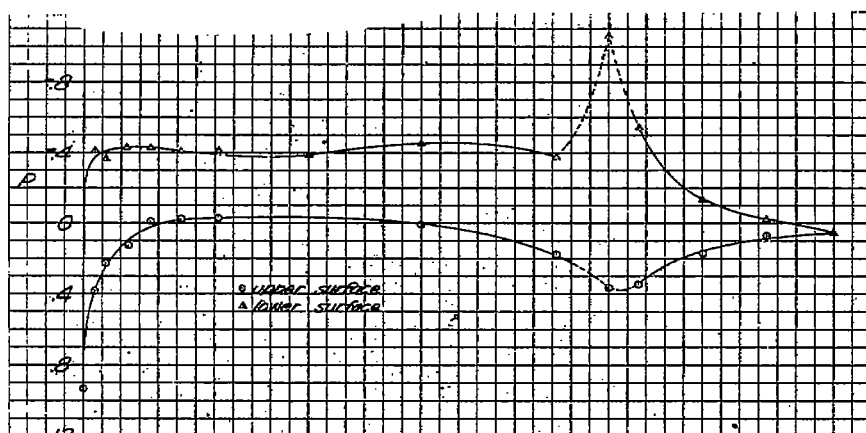
(a) 18-inch station
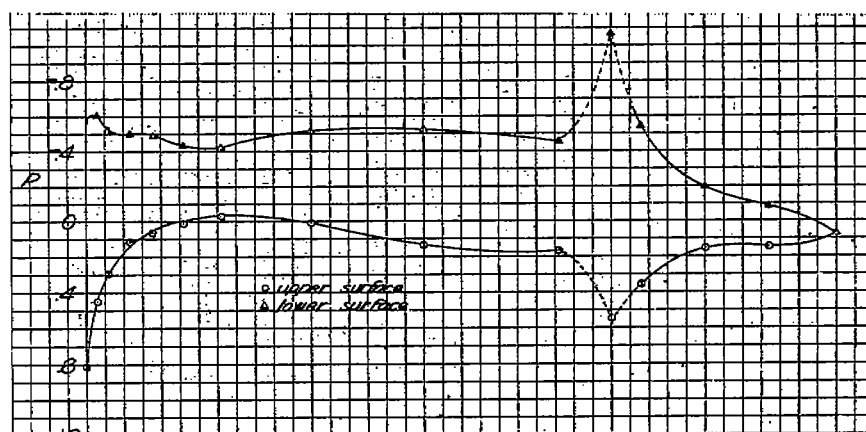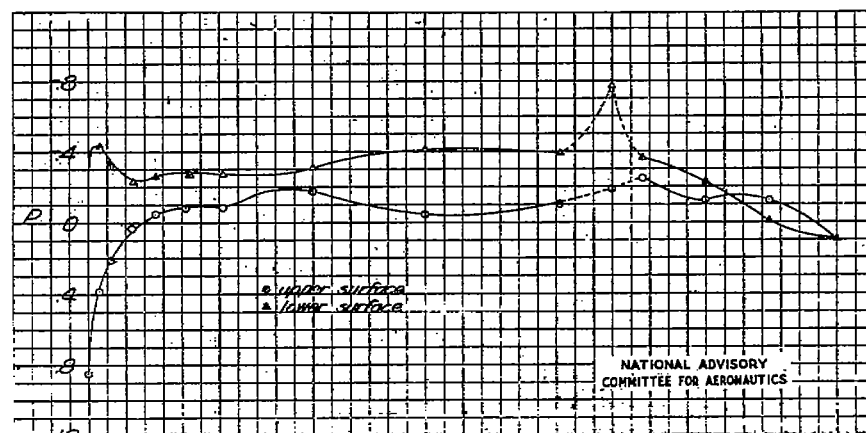
(b) 47.5-inch station

(c) 81-inch station
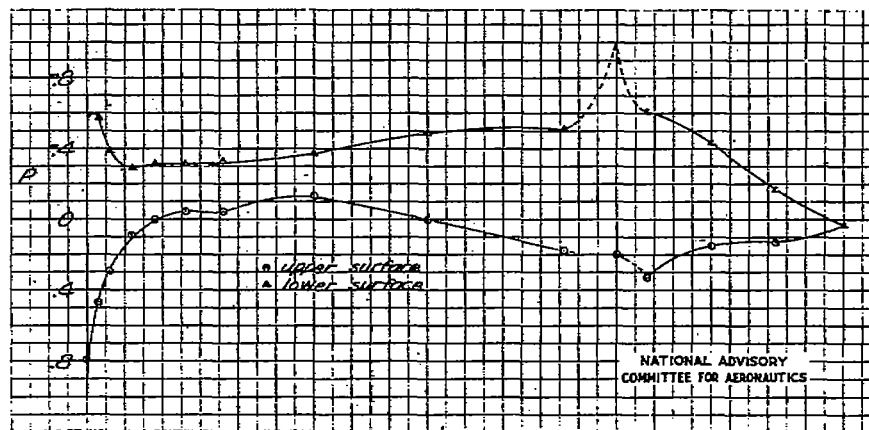
Figure 15.- Pressure distribution at M = 0.20 for $\delta_e = -12.8°$; $\delta_b = 0°$; $\alpha = -0.5°$.
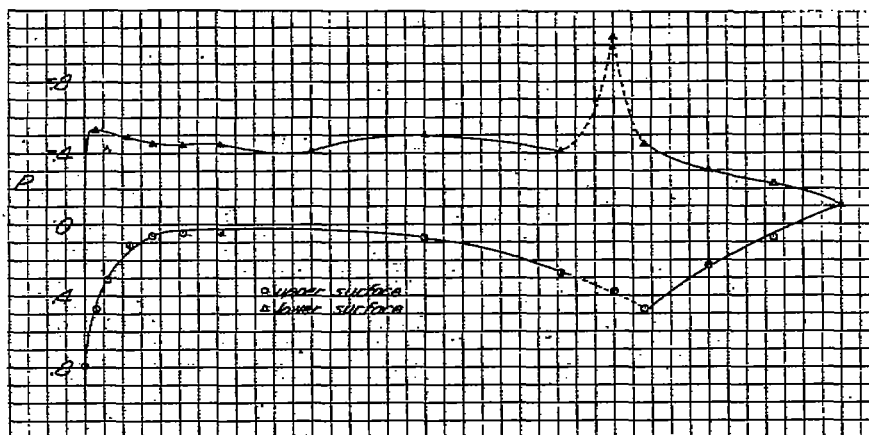
(a) 18-inch station
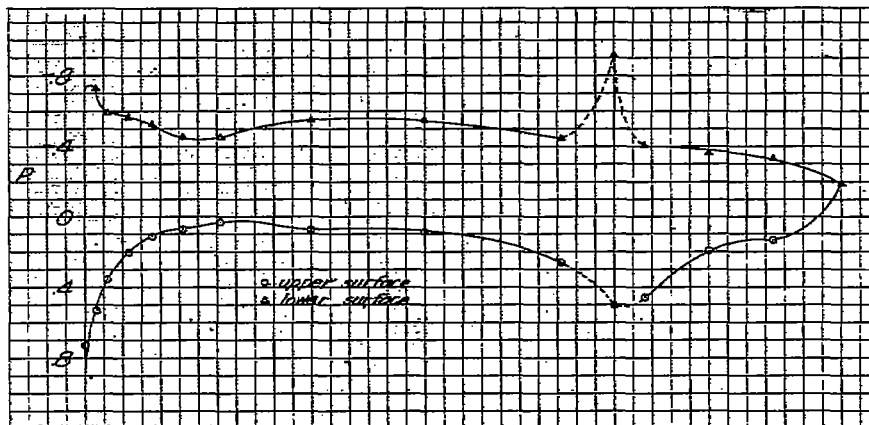
(b) 47.5-inch station

(c) 81-inch station

Figure 16.—Pressure distribution at $M = 0.20$ for $\delta_e = -17.6°$; $\delta_t = 0°$; $\alpha = -0.6°$.

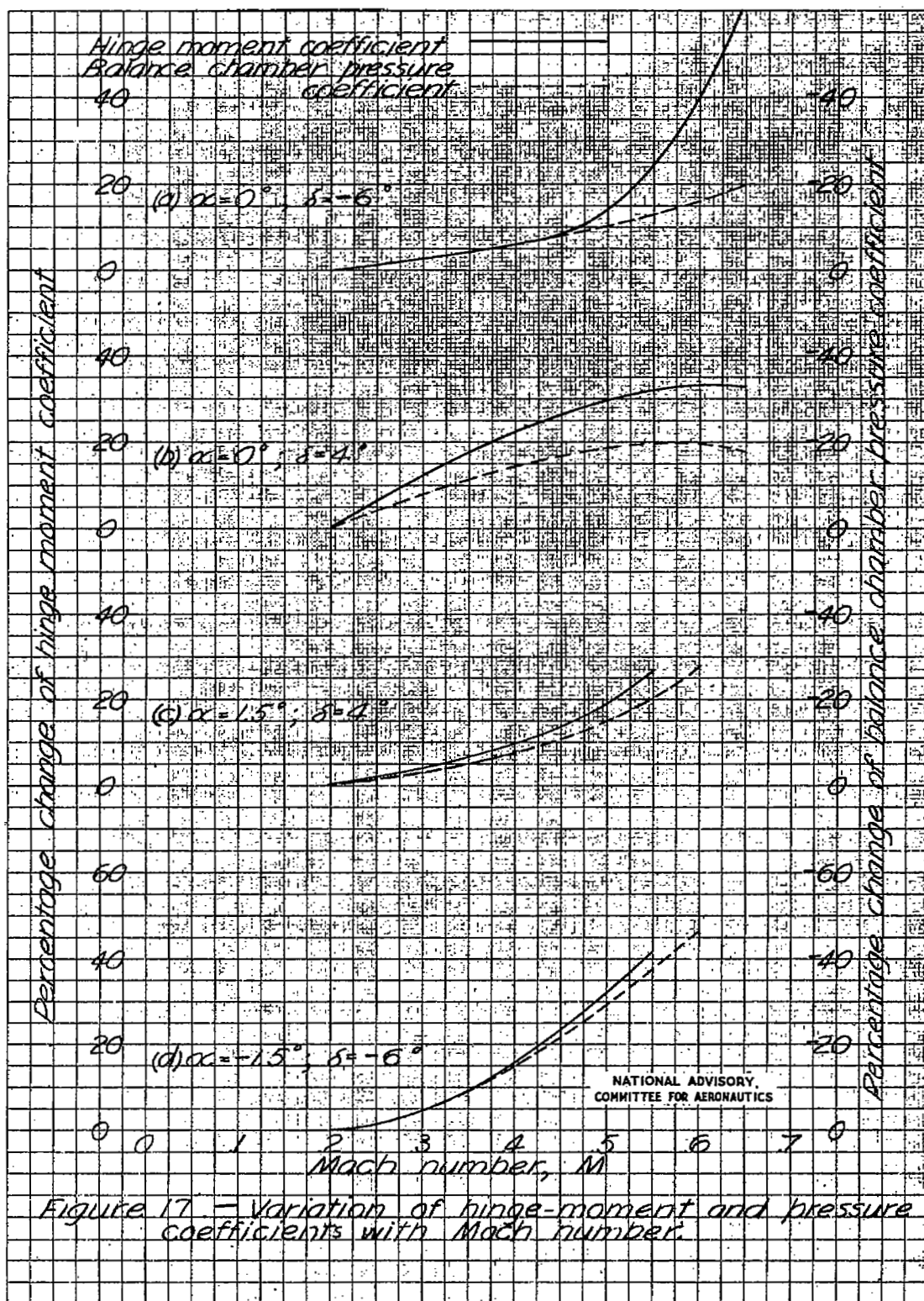Fig. 17   NACA RM No. L7D08

Figure 17 — Variation of hinge-moment and pressure coefficients with Mach number.

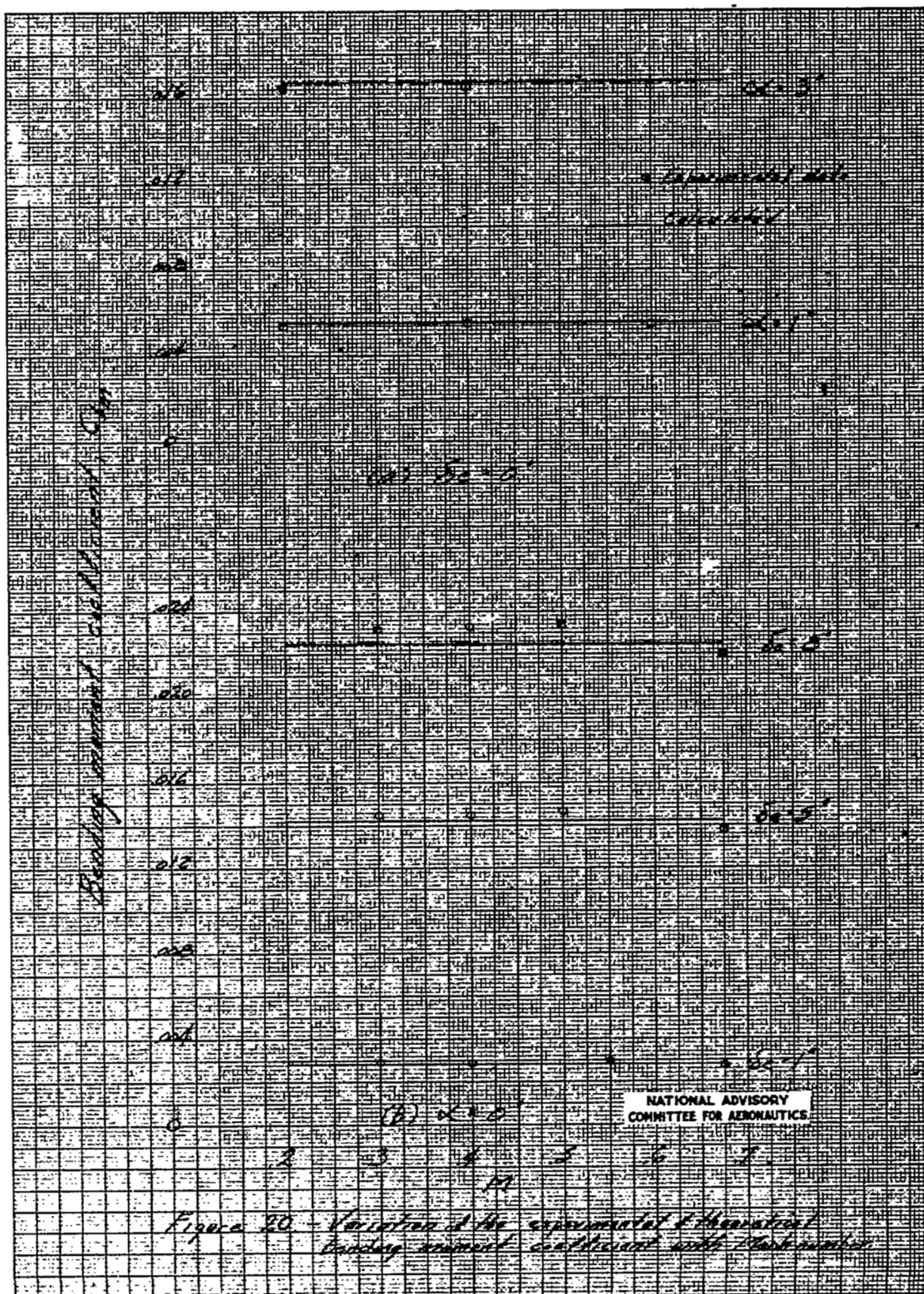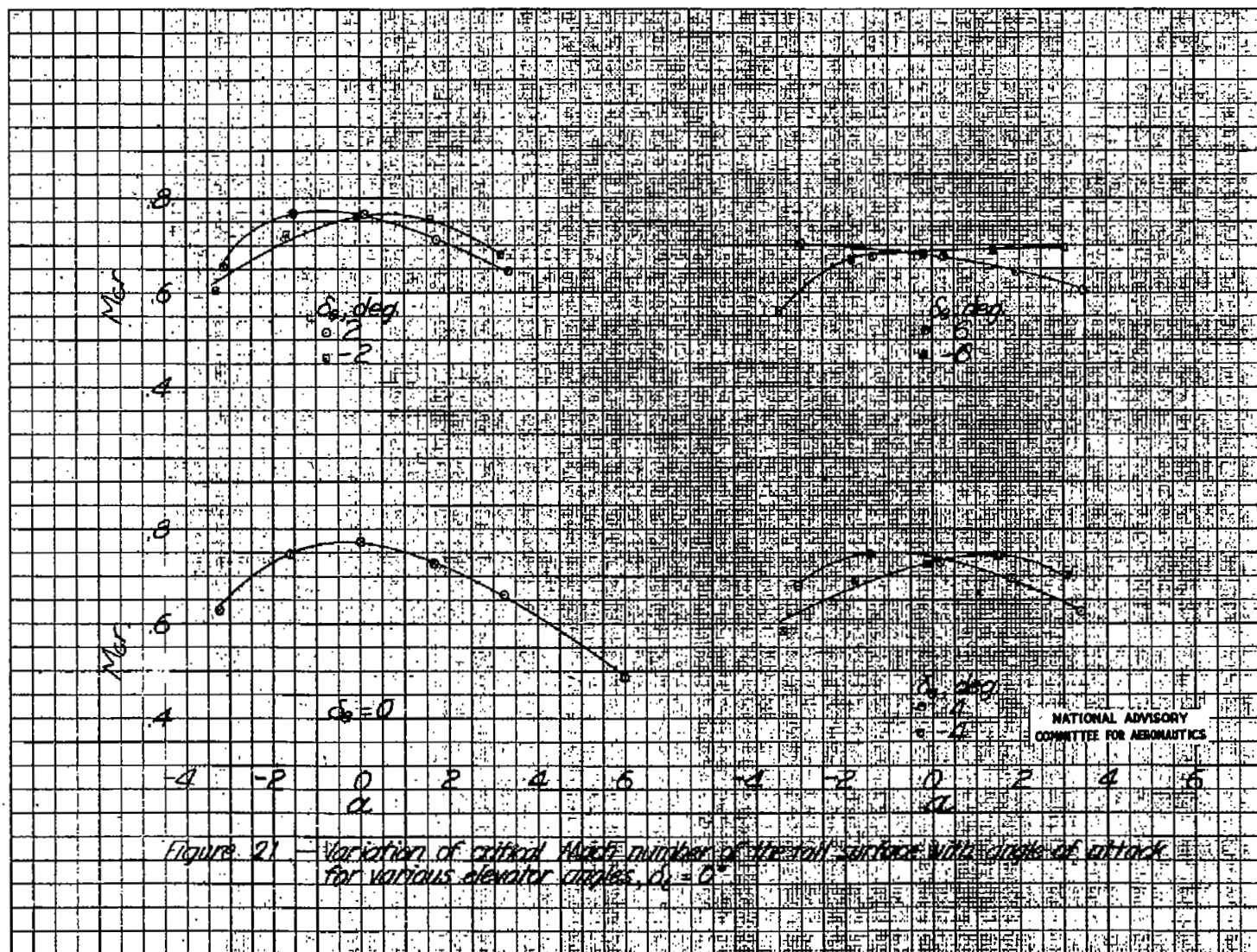Figure 18.— Variation of P_{ac} on the elevator with Mach number.

Fig. 19

Figure 19.— Spanwise variation of the section normal force parameters for various Mach numbers.

Figure 20.- Variation of the experimental & theoretical bending moment coefficient with Mach number.

Fig. 21

Figure. 21 — Variation of critical Mach number of the tail surface with angle of attack for various elevator angles, $\delta_t = 0°$